ASTROBIOLOGY
Volume 20, Number 11, 2020

DOI: 10.1089/ast.2019.2037

The ScanMars Subsurface Radar Sounding Experiment on AMADEE-18

Alessandro Frigeri[1] and Maurizio Ercoli[2]

Abstract

Terrestrial simulations for crewed missions are critically important for testing technologies and improving methods and procedures for future robotic and human planetary exploration. In February 2018, AMADEE-18 simulated a mission to Mars in the Dhofar region of Oman. During the mission, a field crew coordinated by the Österreichisches Weltraum Forum (OeWF) accomplished several experiments in the fields of astrobiology, space physiology and medicine, geology, and geophysics. Within the scientific payload of AMADEE-18, ScanMars provided geophysical radar imaging of the subsurface at the simulated landing site and was operated by analog astronauts wearing spacesuits during extra-vehicular activities. The analog astronauts were trained to operate a ground-penetrating radar instrument that transmits and then collects radio waves carrying information about the geological setting of the first few meters of the subsurface. The data presented in this work show signal returns from structures down to 4 m depth, associated with the geology of the investigated rocks. Integrating radar data and the analog astronauts' observations of the geology at the surface, it was possible to identify the contact between shallow sediments and bedrock, the local occurrence of conductive soils, and the presence of pebbly materials in the shallow subsurface, which together describe the geology of recent loose sediments overlying an older deformed bedrock. The results obtained by ScanMars confirm that subsurface radar sounding at martian landing sites is key for the geological characterization at shallow depths. The geologic model of the subsurface can be used as the basis for reconstructing palaeoenvironments and paleohabitats, thus assisting scientific investigations looking for traces of present or past life on the Red Planet.
Key Words: Mars—Analog—Field test—Geology—Radar. Astrobiology 20, 1338–1352.

Highlights

- The ScanMars experiment brings a ground-penetrating radar to the AMADEE-18 simulated Mars mission.
- The ScanMars radar was operated following procedures and training developed before the mission.
- Approximately 2000 m of radar data profiles have been acquired during the analog mission.
- Combining the results for ScanMars, orbital remote sensing data, and first-person observation in the field while wearing spacesuits (analog astronauts), it was possible to generate a geological model at the AMADEE-18 study site.

1. Introduction

Human exploration of Solar System bodies will include experiments and observations that are currently impossible to implement with orbital remote sensing or robotic missions. Astronauts will have direct contact with a planetary surface, outcrops, and habitats where potential traces of present or past life may exist, operative possibilities that are unreachable through any robotic mission. Currently, most of the very shallow subsurface (first few meters) of Mars remains unexplored, and as has been proven by human missions to the Moon, access to the subsurface by direct sampling and geophysical investigation is critical to understanding the material and sequence of processes involved in the evolution of an extra-terrestrial body (Schmitt, 1973). The nature of rocks and geologic processes throughout time are of primary importance for astrobiological investigations and subsequent sample return missions to Mars.

For this reason, simulated planetary missions that involve fieldwork on terrestrial analog sites (Farr *et al.*, 2002; Osinski *et al.*, 2006; Preston *et al.*, 2014) represent an important activity to prepare and improve the scientific observations and enable us to better understand surface processes on Mars and other planetary bodies (Preston and

[1]Istituto di Astrofisica e Planetologia Spaziali (IAPS), Istituto Nazionale di Astrofisica (INAF), Rome, Italy.
[2]Dipartimento di Fisica e Geologia, Università degli Studi di Perugia, Perugia, Italy.

Dartnell, 2014; Martins *et al.*, 2017; Cavalazzi *et al.*, 2019). In this context, the roles of geological and geophysical studies are fundamental in the following ways: (1) selection of a landing site, (2) assistance in scientific targeting, and (3) a focus on subsurface field campaigns, which, in the case of Mars, is relevant for astrobiological studies as the subsurface is shielded from oxidants and UV and ionizing radiation (Abrevaya *et al.*, 2016; Rossi and van Gasselt, 2018). Survey methods needed for planetary missions should be tested during terrestrial analog exercises (Stoker *et al.*, 2007; Boisson *et al.*, 2011; Hamran *et al.*, 2015), and forthcoming missions to Mars include geophysical imaging and *in situ* subsurface exploration (*e.g.*, Mars 2020, Williford *et al.*, 2018; ExoMars 2022, Vago *et al.*, 2017; De Sanctis *et al.*, 2017; Ferrari *et al.*, 2018).

Fieldwork in hostile environments offers an important opportunity to build experience in terms of protocols, workflows, instrumental performance, and problem-solving techniques, all of which will enrich our knowledge and help to improve the design, operation, scientific analysis, and outcome of future missions (Snook and Mendell, 2004; Cannon *et al.*, 2007; Groemer, 2014; Losiak *et al.*, 2014a, 2014b). Several simulated missions have been developed in the past decade, such as the NASA DESERT-RATS (Abercromby *et al.*, 2013), the NASA HI-SEAS (Binsted *et al.*, 2013; Binsted *et al.*, 2015; Häuplik-Meusburger *et al.*, 2017), the ESA CAVES (Bessone *et al.*, 2015), MOON-WALK (Imhof *et al.*, 2015; Vögele, 2016), MARS-500 (Poláčková Šolcová *et al.*, 2016), and others (West *et al.*, 2010; Steele *et al.*, 2011). Recent analog field campaigns include MARS 160 (Knightly *et al.*, 2018), BASALT (Beaton *et al.*, 2018), PANGEA (Sauro *et al.*, 2018; ESA, 2019), FELDSPAR (Stockton *et al.*, 2017), CANMARS (Caudill *et al.*, 2019; Osinski *et al.*, 2019), and D-MARS (Rubinstein *et al.*, 2019).

AMADEE is a research program handled by the Österreichisches Weltraum Forum (OeWF) and is scheduled between 2018 and 2028. AMADEE-18 (Groemer, 2018; Gruber *et al.*, 2019) follows the OeWF's PolAres program, which included 11 missions simulating the conditions of the Red Planet. PolAres simulations have been under operation since 2006 in diverse terrestrial sites and environments (Groemer *et al.*, 2007, 2014, 2016; Orgel *et al.*, 2014; Dorizon *et al.*, 2016) and were mainly focused on geoscience and astrobiology, with some of them featuring subsurface radar sounding experiments (Groemer *et al.*, 2014, 2016). All of these simulations are aimed toward the reconstruction of geological evolution, astrobiological features, and the assessment of the habitability of martian environments.

The field experiments at Earth analog sites are part of the AMADEE-18 analog mission and support the success of AMADEE program as a whole, with an improvement in understanding the potential of the methods, techniques, and results, such as those presented in this work that describe the ScanMars experiment onboard AMADEE-18 simulated mission in Oman (Groemer *et al.*, 2020 this issue).

1.1. Subsurface radar sounding

The use of electromagnetic waves for geophysical imaging of the subsurface has been under development since the 1970s (Annan, 2002). Similar to seismic imaging, radar echoing returned by impinged signal reveals geological structures beneath the topographic surface. This technique has evolved under the name of ground penetrating radar (GPR) and has been applied to a broad range of studies, including glaciology (Annan and Davis, 1976; Arcone, 1996; Arcone *et al.*, 2005; Bradford *et al.*, 2009a, 2009b; Forte *et al.*, 2013; Godio *et al.*, 2015; Colucci *et al.*, 2016; Del Gobbo *et al.*, 2016; Godio and Rege, 2016; Santin *et al.*, 2019), structural and sedimentary geology (Grasmueck, 1996; Bristow and Jol, 2003; Pipan *et al.*, 2003; Neal, 2004; Ercoli *et al.*, 2012), paleoenvironmental reconstructions (Pellicer *et al.*, 2012; Tillmann and Wunderlich, 2014; Liu *et al.*, 2019), seismotectonics (Liner, 1997; McClymont *et al.*, 2008; Ercoli *et al.*, 2014; Cinti *et al.*, 2015), geotechnical engineering (Liu and Xie, 2013), and archaeology (Daniels, 2004; Jol, 2009; Solla *et al.*, 2011; Ercoli *et al.*, 2016; Kowalczyk *et al.*, 2017; Casas *et al.*, 2018). The GPR represents a powerful noninvasive imaging technique that is capable of collecting data from the subsurface with high spatial resolution in a relatively short time.

1.2. Radars in planetary exploration

Radar sounders, in their orbiting form, have already been successfully deployed to some bodies of the Solar System. In the Apollo era, the Lunar Sounder Experiment was part of the payload of the Apollo 17 mission to the Moon (Porcello *et al.*, 1974). In the 2000s, Italian radar experiments were part of the ESA Mars Express and NASA Mars Reconnaissance Orbiter (MRO) missions to Mars. The Mars Advanced Radar for Subsurface and Ionosphere Sounding (MARSIS) and the Shallow Subsurface Radar (SHARAD) have characterized the geology of the martian icy layers (Picardi *et al.*, 2005; Plaut *et al.*, 2007; Seu *et al.*, 2007; Phillips *et al.*, 2008; Orosei *et al.*, 2018). SELENE's Lunar Radar Sounder onboard the Japanese Kaguya mission to the Moon has been used for characterizing the lunar regolith (Ono *et al.*, 2008). The CONSERT experiment onboard the ROSETTA mission to comet 67P/Churyumov-Gerasimenko was a bistatic radar used for probing the nucleus of the comet (Kofman *et al.*, 2015). Radar sounders are also planned in future missions. The Radar for Icy Moon Exploration (RIME) (Bruzzone *et al.*, 2013) onboard the JUpiter ICy moons Explorer (JUICE) mission will provide orbital subsurface sounding for the icy crusts of Ganymede, Europa, and Callisto. Since the 1990s, GPR has been studied as a possible part of a scientific payload on a planetary robotic mission (Grant and Schultz, 1992; Grant *et al.*, 2003). The Chang'e-3 robotic mission accomplished the first GPR survey on the Moon (Fang *et al.*, 2014; Su *et al.*, 2014; Ding *et al.*, 2020).

NASA's Mars 2020 and ESA's ExoMars 2022 will be the first two robotic missions operating GPR experiments at the surface of Mars. The data returned by Radar Imager for Mars' Subsurface Exploration (RIMFAX, Hamran *et al.*, 2016) and Water Ice and Subsurface Deposit Observation on Mars (WISDOM, Ciarletti *et al.*, 2017) will be critical for knowledge of the first few meters of the martian subsurface, which is protected from damaging radiation and thus the ideal target to preserve past and/or present traces of life (Abrevaya *et al.*, 2016).

2. The ScanMars Experiment

ScanMars was proposed in response to the announcement of opportunity launched by OeWF in the summer of 2017. The submitted idea aimed at accomplishing shallow subsurface geophysical imaging of arid environments at the analog landing site by including a GPR experiment into the scientific payload of AMADEE-18. In contrast to common GPR campaigns, where experts operate and have direct access to the instruments, ScanMars experiment will train the analog astronauts, who are not field geophysicists, to operate the radar when wearing spacesuits during the extravehicular activities planned for the mission. Data collected by ScanMars offer the opportunity to extract information on the geological setting, including the presence of water or structures related to past or current activity, similarly to the subsurface investigations on Mars made at the global scale by the orbital planetary subsurface radar sounders MARSIS and SHARAD (Seu *et al.*, 2004; Picardi *et al.*, 2005; Plaut *et al.*, 2007, 2009; Stuurman *et al.*, 2016; Orosei *et al.*, 2015). Orbital subsurface-penetrating radars offer global coverage and a penetration depth of several hundred meters with a resolution of tens of meters, whereas surface GPR returns data from the first few meters of the subsurface with a spatial resolution that is capable of imaging geological structures and layers down to a few centimeters. In this perspective, GPR experiments are well suited for the scale of observations that are common in robotic and human landed missions.

In July 2017, ScanMars was selected to be part of the AMADEE-18 mission, which is scheduled for February 2018 in the Dhofar region of Oman. The experiment includes the instrument, training of the analog astronauts, and planning the observations from available remote-sensing data. These single elements were put together to run the ScanMars experiment. The instrument used for the ScanMars experiment consists of a commercial GPR Zond-12e manufactured by Radsys, Latvia. Among the commonly used antennae operating from tenths of megahertz to a few gigahertz, we chose an operative frequency of 500 MHz as a good compromise between spatial resolution, penetration depth, and maneuvrability of the antenna on the field. Lower frequencies would penetrate deeper in low-loss media at the expense of lower spatial resolution. In addition, the larger physical dimensions of the antenna would be impractical for the astronauts in spacesuits. On the other hand, higher operative frequencies up to 1–2 GHz offer a very compact antenna system and higher spatial resolution, but the reduced penetration of the signal ($\sim$50 cm; Annan, 2001) would preclude the detection of geologic structures and layers beneath the soil.

With the selection of a 500 MHz antenna for ScanMars, we expected a penetration depth up to 10 m with a vertical resolution of a few centimeters, which enables the detection of features that would be impossible to identify from surface observations. An odometer was applied to the antenna sled, and the wheel was programmed to trigger the data acquisition every 2 cm along the antenna path, setting the horizontal spatial resolution of the survey.

The pre-mission phase involved the production of procedures and their testing during the training rehearsal with the analog astronauts and the field crew. A few weeks before the mission, we had access to remote-sensing data of the landing site and started planning possible observation targets. The available remote-sensing data comprised an image mosaic in the visible range at a resolution of 0.5 m per pixel and a 5 m per pixel Digital Terrain Model (DTM). Geospatial data were served through an internet connection by the OeWF geospatial server offering Open GIS Consortium interoperable web services and accessed remotely by the Geographic Information System software QGIS (QGIS Development Team, 2020). Accessing these datasets over the internet, it was possible to quickly select scientific targets and plan possible ScanMars profiles (transects), which were then submitted to the science operations team and included in the mission schedule.

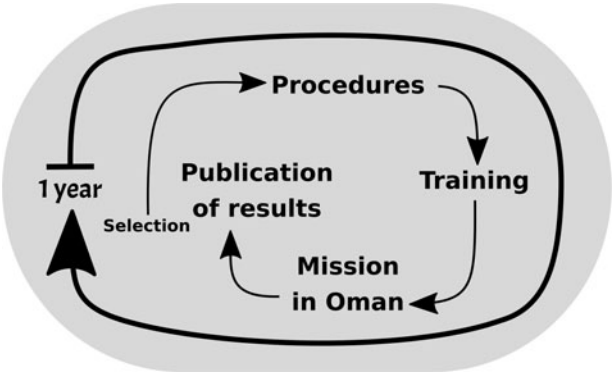

FIG. 1. The ScanMars on AMADEE-18 lifecycle and timeline. After the selection of the experiment, the scientific team produced the Standard Experiment Information document (SEIF, see Fig. 2) describing the operational aspect of the experiment, and has been included in the field-crew training material. The face-to-face training offered the opportunity to review the procedures and to operate the instrument in first person by the field-crew supported by the field geophysicists. After the simulated mission in Oman, the publication of the results starts about one year after the selection process.

During the mission phase, the field crew acquired data following instructions from the mission support room. At the end of each day of extra-vehicular activity (EVA) ScanMars operations, data were saved at the base station and transmitted back to the mission control at OeWF in Innsbruck and archived as raw data. As soon as the raw data were made available on the mission server, a cycle of processing and interpretation by the scientific team transmitted feedback on the data quality and contents to the base station, so the field crew was able to proceed with the program.

In the post-mission phase, data were processed more accurately and re-interpreted and archived.

Figure 1 shows the timeline of the experiment, from the selection of the experiment to the deployment of the mission. The whole process lasted $\sim$1 year, which allowed the program to keep its very high rhythm of mission cycles, of one AMADEE expedition approximately every 2 years.

2.1. The development of procedures and training

The AMADEE-18 field crew did not include a field geologist or an expert in GPR data acquisition. In this scenario, the procedure and training of mission personnel

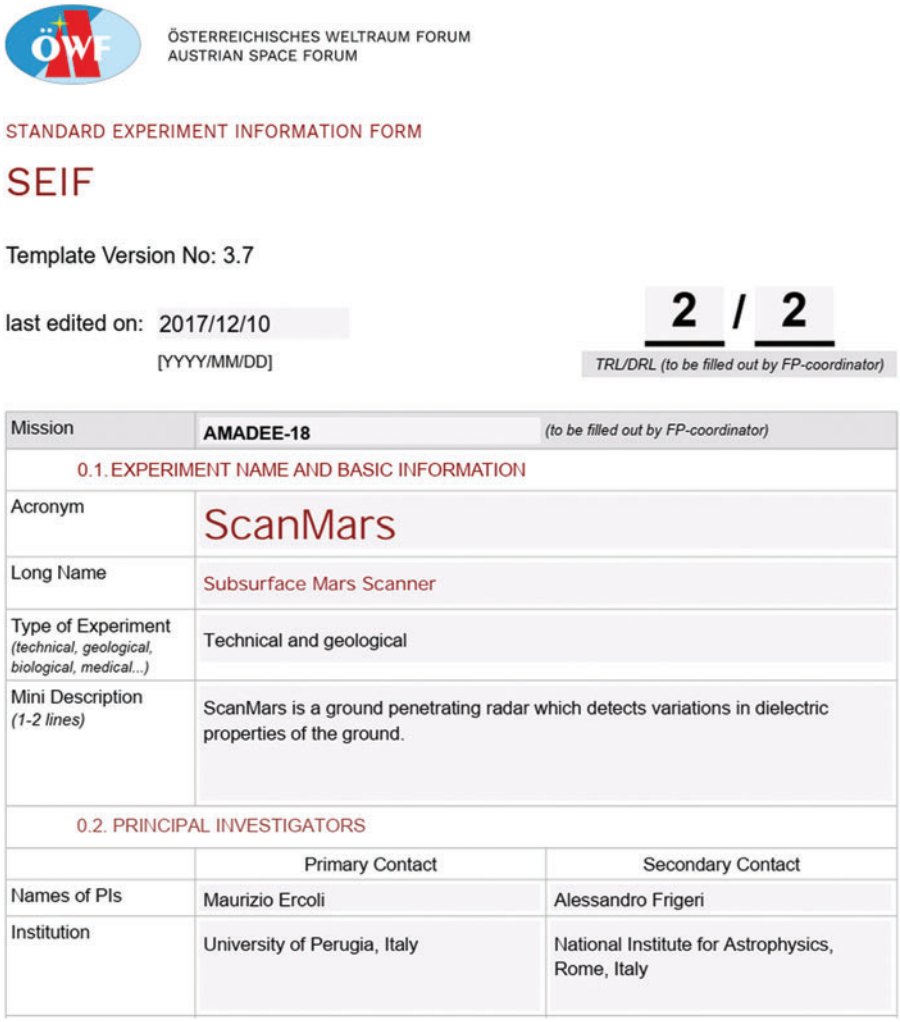

ÖSTERREICHISCHES WELTRAUM FORUM
AUSTRIAN SPACE FORUM

STANDARD EXPERIMENT INFORMATION FORM

SEIF

Template Version No: 3.7

last edited on: 2017/12/10
[YYYY/MM/DD]

2 / 2
TRL/DRL (to be filled out by FP-coordinator)

Mission	AMADEE-18	(to be filled out by FP-coordinator)
0.1. EXPERIMENT NAME AND BASIC INFORMATION		
Acronym	ScanMars	
Long Name	Subsurface Mars Scanner	
Type of Experiment (technical, geological, biological, medical...)	Technical and geological	
Mini Description (1-2 lines)	ScanMars is a ground penetrating radar which detects variations in dielectric properties of the ground.	
0.2. PRINCIPAL INVESTIGATORS		
	Primary Contact	Secondary Contact
Names of PIs	Maurizio Ercoli	Alessandro Frigeri
Institution	University of Perugia, Italy	National Institute for Astrophysics, Rome, Italy

FIG. 2. The title page of the Standard Experiment Information Form (SEIF) document for the ScanMars experiment, which includes the description of the radar equipment and its components, the step-by-step assembly and disassembly and operative instructions. This document has been the base for preparing the training and has been the reference manual during the simulated mission in Oman. Color images are available online.

becomes a critical part of the ScanMars experiment, which was operated in the field by personnel without previous experience in geophysical field data acquisition. Figure 2 shows the first page of the Standard Experiment Information Form (SEIF), which includes information about the instrument and operational procedures, from hardware setup to software operations. After an iteration of incremental revisions, the final SEIF document was delivered to the AMADEE-18 field crew, including the ScanMars instructions in their main training program. Technical terminology for GPR surveying needed to be explained and simplified as much as possible to make the SEIF usable by the crew. The training phase was then concluded at the OeWF headquarters in Innsbruck, where a face-to-face meeting was conducted to review topics related to radar principles, share questions, and review the procedures together with the field crew. During the training at OeWF, the field-crew team faced practical aspects of experiment deployment, for example, instrument assembly while wearing spacesuit gloves as shown in Fig. 3 or learning the correct force and speed to be applied to the antenna sled during the data acquisition. The field crew and the analog astronauts directly experienced the acquisition of radar data on the ScanMars display and were taught how to set up the main instrument parameters required to operate the radar correctly during EVAs. Examples of data acquisition cases that showed acceptable to very bad or no data acquisition, or data artefacts, were given to the crew to facilitate the detection of possible problems in the field.

2.2. Survey design and planning

The landing site of AMADEE-18 is in south Oman. The astronauts surveyed a desert area where dry riverbeds alternate with erosive surfaces and ancient marine sediments. The flat surfaces are part of the Shuram Formation, in the form of siliciclastic cohesive surfaces (Searle, 2019). The Shuram Formation was deposited in the shallow water of a marine platform and dates between Late Precambrian and Early Cambrian (Gorin *et al.*, 1982). The geology of the area is characterized by the alternation between old marine units and more recent continental water-related deposits and structures. We planned observations that would cross dry fluvial sediments in search of water-related geologic features. A more extensive geology review and a reference geological map of the study site are available in the mission overview and laboratory analysis contributions of this issue (Groemer *et al.*, 2020; Lalla *et al.*, 2020).

FIG. 3. ScanMars training. The analog astronaut trainee is testing operative procedures during the training at OeWF headquarters in Innsbruck, Austria. A commonly simple task like the assembly of the odometer on the antenna sled becomes challenging when it has to be done with spacesuits' gloves. The face-to-face training offered the opportunity to enrich the operational procedures with first person experience on the instrument hardware. Color images are available online.

2.3. Data acquisition

The AMADEE-18 experiments were deployed after the simulated mission began in February 2018. ScanMars was operated during EVA by two astronauts, one pulling the antenna system and the other holding the radar processing unit with a display that showed the operative parameters and a preview of the data being acquired (Fig. 4). The location of the planned transects stored in the mission's Geographic Information System (GIS) was converted into coordinates that the astronauts were able to follow by using GPS. The astronauts were commanded by the flight-control room and driven to target locations. The analog astronauts acquired ScanMars data over five different designated areas for a total of $\sim$2000 m of profiles collected during the whole mission. A total number of 22 bidimensional GPR profiles, corresponding to about 85,000 radar traces, were recorded and archived. Each trace comprises 1024 samples, spaced by 0.195 nanoseconds. Profile elevation along the ScanMars transects was extracted from the DTM (5 m per pixel resolution, available from the mission's GIS), from the start/end GPS coordinates of each transect. The scientific team had access to the data on a daily basis to check its quality and communicate or discuss any anomalies with the remote science support team, giving an opportunity to update the procedures between sessions when needed.

2.4. Processing flow

GPR is a high-resolution geophysics imaging technique that requires a processing strategy commonly dictated by the survey goal and the nature and complexity of the terrain being investigated; therefore, it is not possible to identify a standard processing pipeline.

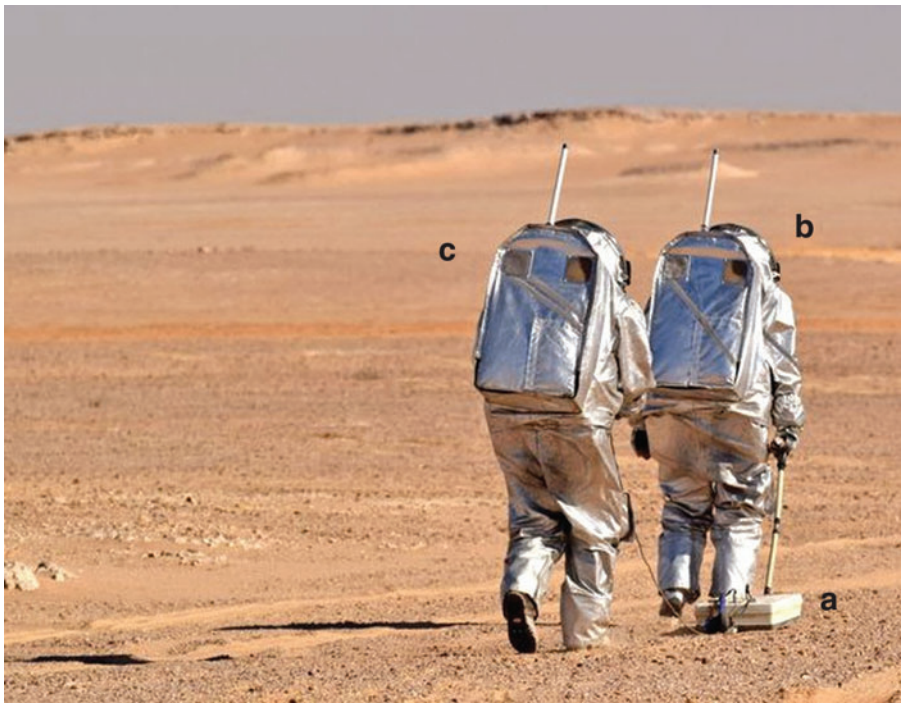

FIG. 4. ScanMars operations during an Extra Vehicular Activity (EVA). The radar antenna sled **(a)** is being pulled along the planned transect by astronaut **(b)**, while a second one **(c)** carries the Central Processing Unit (CPU) which displays a live view of the data being acquired along with the operative parameters of the instrument (picture credits OeWF). Color images are available online.

For our processing of ScanMars data, we used the ReflexW software to design and save a customized processing flow (Jol, 2009). This also improved the signal-to-noise ratio of the data (*e.g.*, removing unwanted noise components) and restored a reliable geometry to the reflections (*e.g.*, real dip of reflectors and collapse of hyperbolic diffractions; Davis and Annan, 1989; Fisher *et al.*, 1992). The processing flow we chose for ScanMars data is composed of 12 steps, which are applied in sequence:

Raw data editing and merging of geographic coordinates: Original data are reviewed visually, and possible problems in data are fixed. The geometry of the acquisition is reconstructed and applied to the raw data.

Dewow, time-zero correction: High-pass filtering, which removes DC current effects, and first impulses are aligned on to each other (Annan, 1999).

Amplitude recovery: A gain curve is applied to the signal to compensate for energy losses with depth. In this ScanMars workflow, we applied a combination of linear and exponential functions (Annan, 1999).

2D average subtraction filter: Horizontal banding among signals is removed by a moving window filter.

Spiking deconvolution: Compresses the wavelet in the time domain, broadening the spectrum in the frequency domain (Yilmaz, 2001), resulting in an improvement in time resolution.

Background removal: Removes the mean of all traces to each trace (Annan, 2002). It is applied to attenuate ringing effects introduced by the spiking deconvolution filter.

Butterworth bandpass filtering: The combination of high-pass and a low-pass filter to remove noise at a frequency higher and lower than effective bandwidth, which is usually lower than the nominal one due to the down-shifting effect of the terrain (Butterworth, 1930; Yilmaz, 2001).

F-K (Stolt) migration: The migration process traces back the reflection and diffraction energy to their source points. This specific migration corrects for the distortions due to signal propagation (Stolt, 1978), developing more spatially realistic subsurface images.

Average 2D filter: Smoothing filter suppresses high-frequency noise. Usually, it emphasizes geologic layers providing more continuity.

Time cut: The time range is trimmed up to the point where the signal is not usable anymore due to a very low signal to noise ratio.

Topographic (static) correction: The time delay of each trace is shifted by using a constant velocity to account for the elevation changes (Yilmaz, 2001) extracted and interpolated by using the GIS transect.

Time-to-depth conversion ($v = 0.1$ m/ns): The traces in two-way travel time are converted into depth by a constant velocity estimate by hyperbola fitting.

This processing pipeline has been applied to all the ScanMars data acquired during the mission.

3. Results

We report here the results of our data analysis on two ScanMars profiles, n. 30 and n. 31. Measurements were made over one of the scientific target areas suggested in the planning phase, located at the contact between alluvial deposits and massive rocks that form the relief. Figure 5 shows imagery and topography of the study area with the location of the traces along which ScanMars radar profiles have been acquired. Profile n. 30 passes across the gently sloping alluvium deposits in the south-western sector of the site

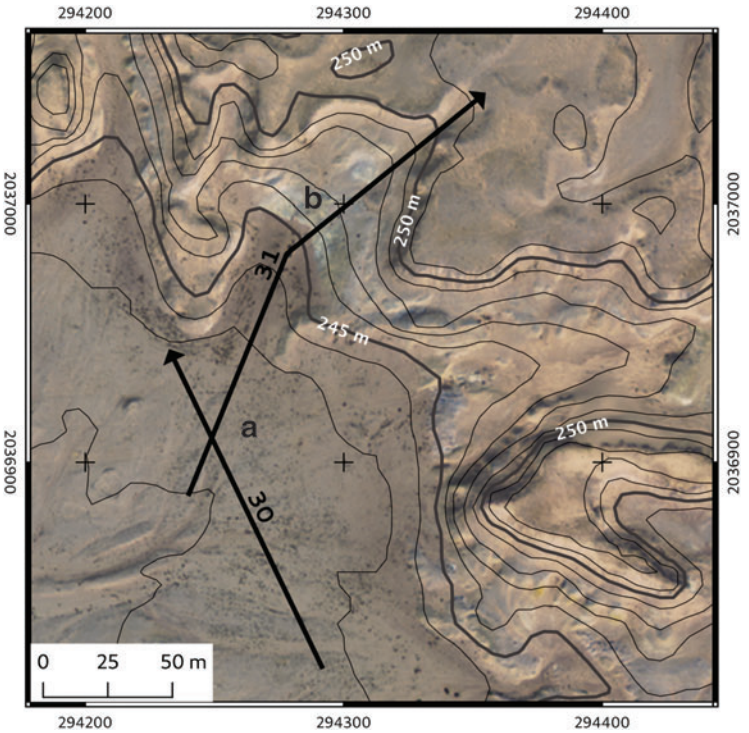

FIG. 5. Context map of the AMADEE-18 scientific target site presented in this work, showing the location of ScanMars profiles 30 and 31. Arrows indicate the direction of acquisition along the trace. Base-map is the 0.5 meters per pixel satellite image showing color variations of the terrain, while topography is represented by elevation isolines at 1-meter interval (data from National Survey Authority, Sultanate of Oman). From the analog astronaut's communication log we extracted the description of surface given at point **a:** *Sandy terrain with poorly sorted rocks with average size around 20 cm* and at point **b:** *bright terrain, rocky outcrop.* Color images are available online.

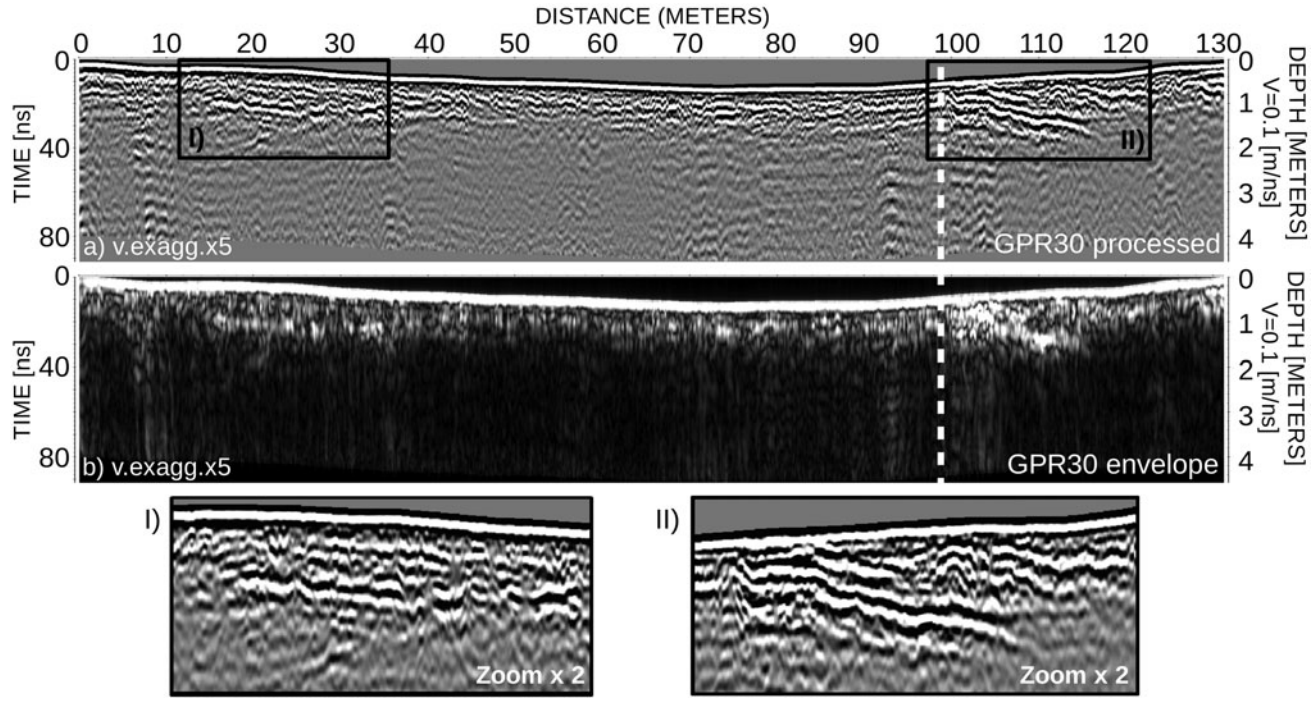

FIG. 6. ScanMars data acquired along profile n°30 (see map in Fig. 5). Radar traces have been processed as described in the text and displayed in greyscale as amplitude **(a)** and its envelope **(b)** (see text for the description). The horizontal axis indicates the distance from the start of the profile, and the vertical axis is the time delay (left) and depth (right) of radar echoes. Panels **I)** and **II)** zoom on parts of the radargram showing bright reflections from the contact between the bedrock and the loose deposits. The white dashed line indicates the intersection with ScanMars profile n°31.

(Fig. 5, point a), whereas profile n. 31 starts in the alluvium, crosses profile n. 30, and ramps upslope across a bright outcrop (Fig. 5, point b), ending on the plateau at an elevation of about 6 m above the floodplain. The lengths of profiles n. 30 and n. 31 are 130 and 200 m, respectively.

Figure 6 shows the data collected along profile n. 30. GPR echo returns acquired along profiles are commonly represented side by side in the form of a radargram, where the horizontal scale indicates the trace number or the distance along the profile, and the vertical scale is twice the travel time, which corresponds to the depth, given an average propagation speed (we used 0.1 m/ns). This visualization gives an opportunity to observe a vertical bi-dimensional variation of reflections and diffraction patterns of radar echoes, or *radar facies* (Huggenberger, 1993; Beres *et al.*, 1999), which can be associated with different geological terrains and structures.

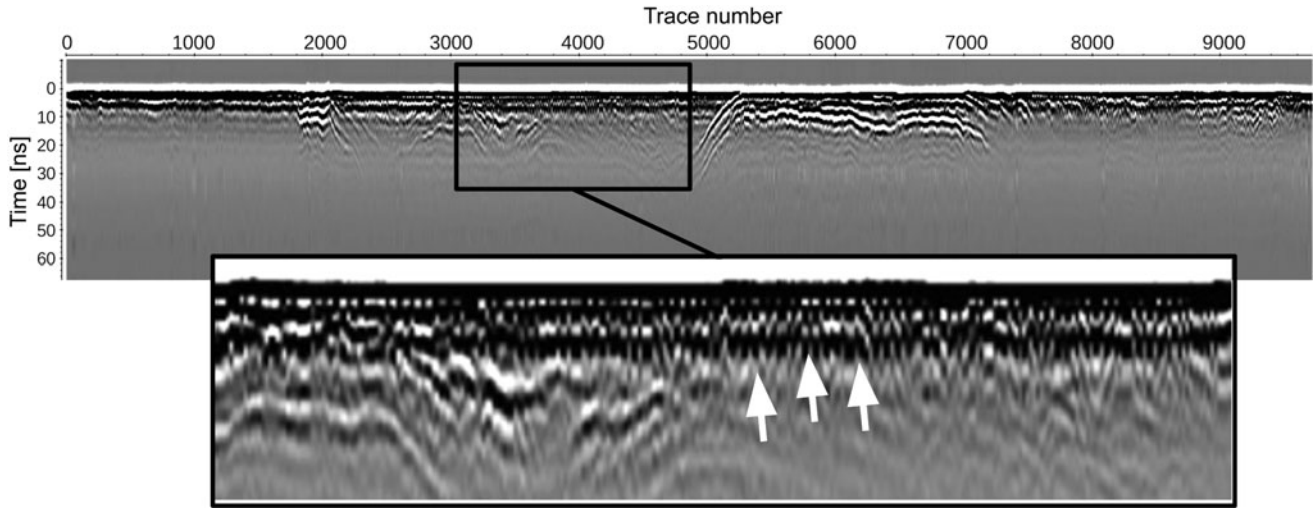

FIG. 7. ScanMars data acquired along profile n°31 (see context map of Fig. 5). The horizontal axis reports the trace number and the vertical axis is the Two-Way-Travel time (TWT) of the radar echoes. The black frame indicates the extent of the magnified part of the radargram showing the *radar facie* associated with the presence of rocks within the loose sediments in the shallow subsurface.

In this work, we display the amplitude of the signals with the classic grayscale (Fig. 6a) and with their absolute value, or *envelope*, which enhances the strongest reflections (Fig. 6b) (Taner *et al.*, 1979; Chopra and Marfurt, 2008; Forte *et al.*, 2012; Zhao *et al.*, 2013; Ercoli *et al.*, 2015). ScanMars profile n. 30 crosses the sandy deposits that cover alluvial terrains, from south-east to north-west. Penetration depth along profile n. 30 reaches 2 m. Two strong reflections are evident on the first half and second half of the profile (Fig. 6a, respectively frame I and frame II). Radar reflections are generated by the contrast of the dielectric properties of the terrains, which may correspond to a change in the composition of rocks/deposits, a change of the geometric setting of the materials, or a combination of both. In this case, we relate the very bright reflections of Fig. 6a panel I and II to the contact between the shallow loose deposits and the bedrock. The latter is exposed at the surface in the hilly terrain and, from remote sensing imagery, appears brighter than the other materials (see Fig. 5, point b). The lack of a distinct reflection in the central portion of this profile may be related to signal attenuation due to the presence of conductive minerals in the sediments, for example, an enrichment in clays. Another reason for the missing reflection from the bedrock in the central part of the radargram may be due to an increase of sediment thickness that resulted in attenuation of the detectable signal under the noise level.

Figures 7 and 8 show ScanMars data from profile n. 31. For this radar profile, it was possible to associate analog astronauts' observations reported from the field during the geophysical data acquisition, describing the type of terrains at the surface. From the astronauts' communications log, it was possible to describe the surface at location ''a'' of Fig. 5 as follows: ''a flat surface made by sandy soil, with some sparse poorly sorted rock pebbles concentrated in the first part of the profile,'' whereas the bright material at point b is reported as ''a totally rocky part at the beginning of the hill.'' Figure 7 shows a detail of the raw data with its diffraction pattern, or *radar facies*, which is typically originated by small rocks at the surface and shallow subsurface (down to a depth of 1 m) correlated to the description of the surface at site ''a'' next to the base of the sloping terrain.

Figure 8 reports the processed profile n. 31, shown in grayscale (Fig. 8a) and with the envelope attribute (Fig. 8b). Panel I shows a detail of the radargram that corresponds to outcrop ''b'' described in the astronauts' communication log. In this zone, the radargram shows curved reflectors following the concave topography and continuing under the surface reflection. These radar data are correlated with a rocky antiform structure exposed along the topographic profile, being covered

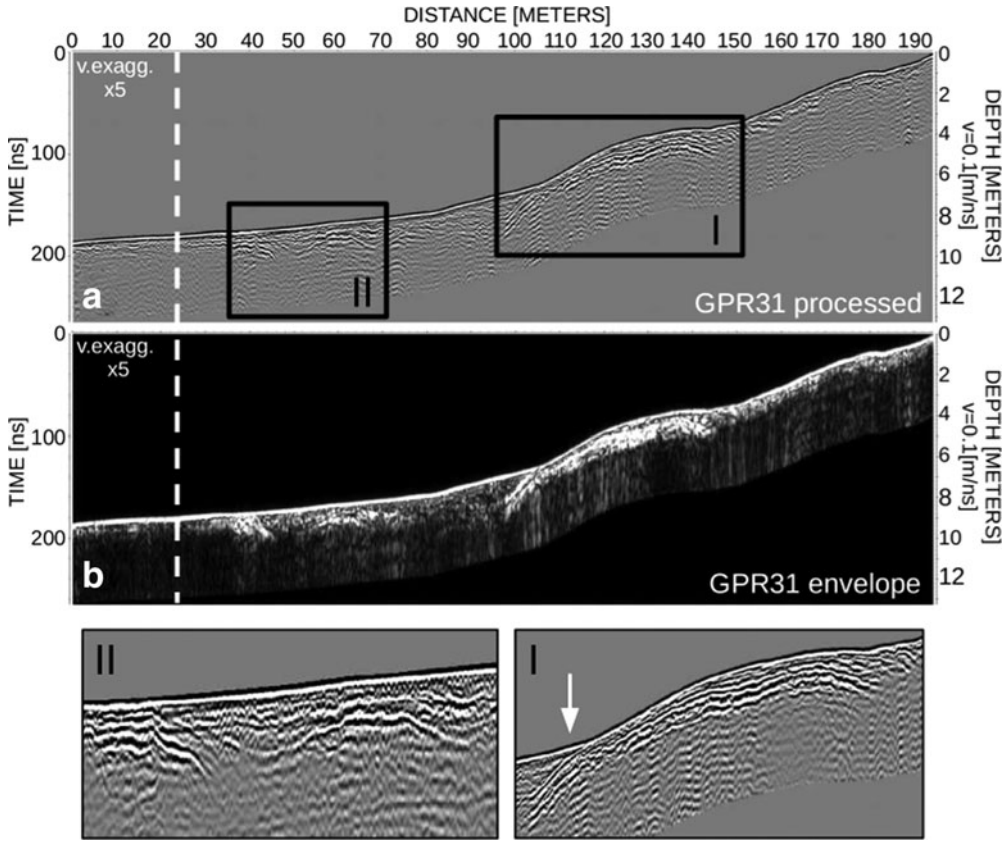

FIG. 8. Processed profile n°31, reported in distance versus depth. **(a)** The radargram corrected for topographic variations. The white dashed line indicates the intersection with profile n°30. **(b)** The envelope attribute display of the radargram enhances the strongest reflections. Panels **I** and **II** show details of the radargram with reflections generated by the interface between the loose deposits onlapping over the bedrock. Panel **I** shows the signals we have associated to an antiform structure outcropping along the profile and extending below the surface; the white arrow indicates the onlap between the loose deposits and the dipping bedrock layers. Panel **II** shows curved reflectors associated to the bedrock and the very dense pattern of reflection from the rocks in the sediment.

by layered sediments at the brake of the slope indicated by the white arrow in Fig. 8, panel I. Panel II shows a curved reflector and a dense pattern of shallow reflections, typically generated by small pebbles in the shallow subsurface (also detectable as dense small diffractions in unmigrated profiles), similar to the same *radar facies* observed in profile n. 30. The curved reflector in panel II is very likely generated by the contact between the bedrock and the overlying pebbly terrain, but in this case the bedrock is not outcropping.

Figure 9 reports the geological cross-section created by the combined interpretation of the radar data, field notes, photographs taken in the field by the analog astronauts, and satellite remote-sensing imagery. The geologic cross-section shows three different units, their boundaries, and their stratigraphic relationship. The lowermost unit is the layered rocky bedrock that shows the major antiform structure outcropping along the profile and minor buried structures in the first part of the profile. An angular unconformity separates the sandy-pebbly sediments (Fig. 9, photo 2) from the underlying bedrock (from 40 to 100 m and from 140 to 160 along the cross-section of Fig. 9). The sharp edges of the pebbles shown in the photographs suggests that they have been generated locally from the erosion of bedrock material or some other rocky unit topographically more elevated and emplaced by gravitational deposition or rapid flooding. The uppermost unit is made by sand (Fig. 9, photo 1), which occurs at the base of the slope. The contact between the sand and the pebbly terrain is not clearly detectable from radar data or documented in the field, but these sediments are probably the most recent of the three.

The geological processes associated with the emplacements of the units described earlier are, in sequence: (1) the compressive deformation of the bedrock, (2) the gravity- or flash flood-driven deposition of the pebbly sands, and (3) the aeolian deposition of sands at the base of the slope.

The morphology shown by remote-sensing data in Fig. 5 suggests that water had an important role in shaping the landscape of this area. Although we did not find evidence of signals generated from the water table, we cannot rule out its presence below the investigation depth of our survey.

The geometric setting and spatial relationship between the signals of the two radar profiles can be visualized in a three-dimensional environment. Figure 10 reports a visualization seen from the north-west of the two ScanMars profiles and their crossing point, showing the geometries of the signals associated with the subsurface geology, including the antiform outcropping along the topographic profile, the loose infills at the base of the scarp, and the layers at the intersection of the profile.

4. Discussion

The dataset returned from the ScanMars experiment presented in this work explored the subsurface of one of the AMADEE-18 scientific target sites down to a depth of 4 meters, showing a wide range of different signal returns. The interpretation of GPR *facies* applied in our work provides a way to classify different sedimentary terrains and structures, and their geometrical relationships within the volume of the rocks explored by the survey.

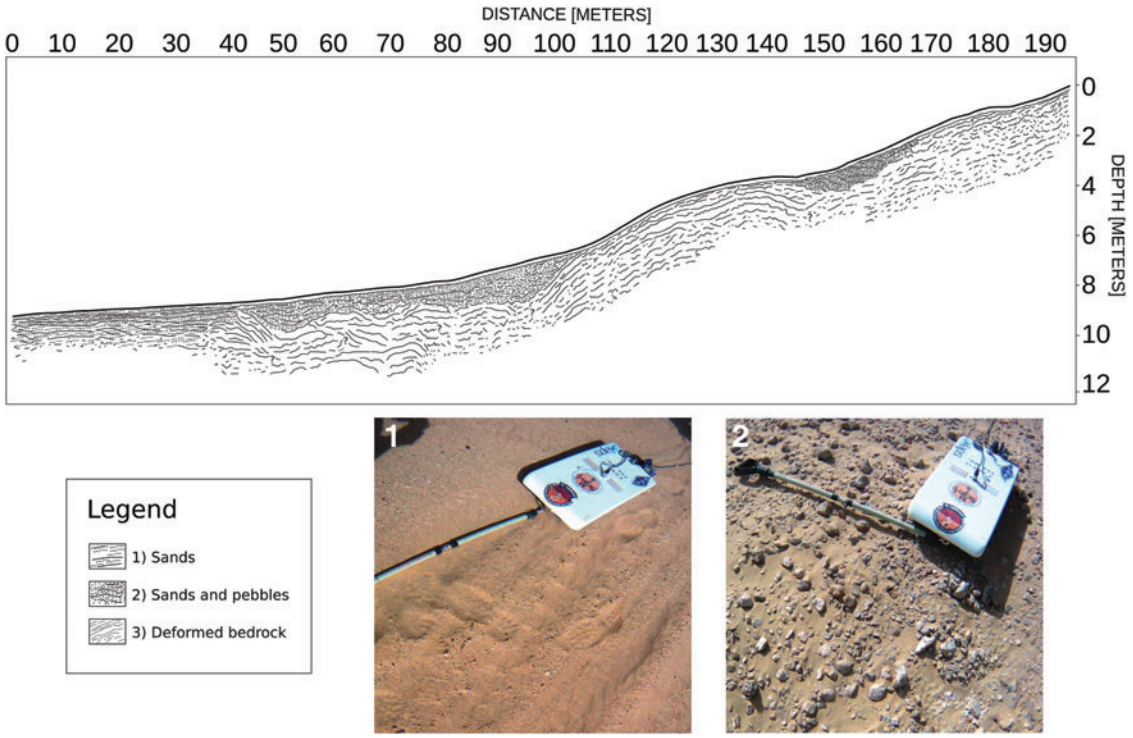

FIG. 9. Geologic cross-section produced from the combined interpretation of radar data, remote sensing data (see Fig. 5) and astronaut observations from the surface along the profile. Pictures **1** and **2** represent the surface exposure of *Sand* and *Sand and Gravels* units. No picture is available for unit 3. The spatial correlation of the units defines the stratigraphic sequence which is the base to reconstruct the geologic evolution of the area (see text). Color images are available online.

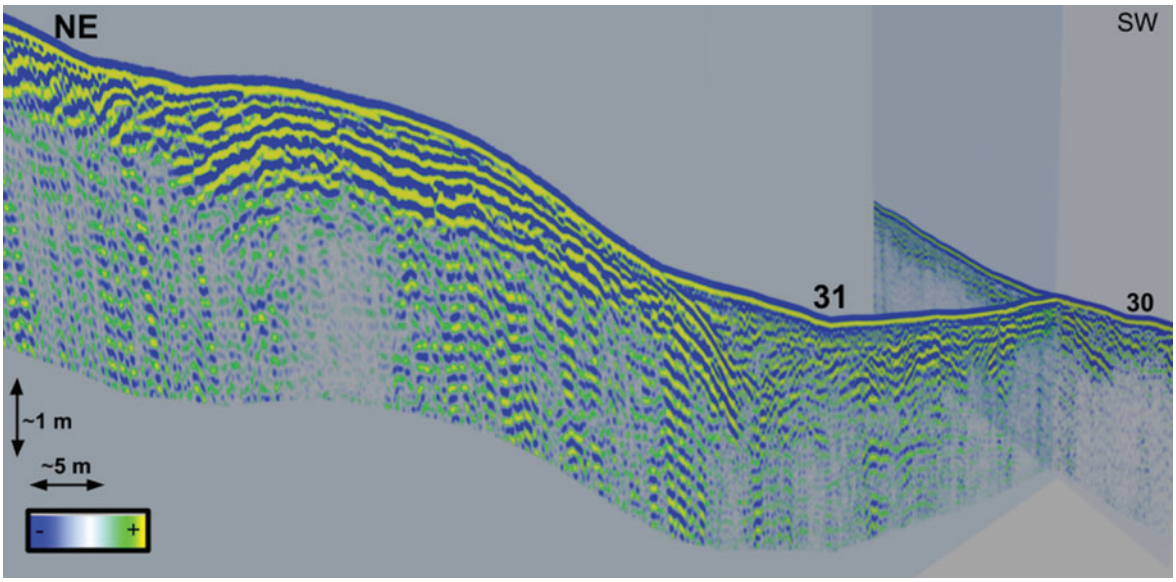

FIG. 10. ScanMars data of profiles n. 30 and 31 visualized in three dimensions. Color scale indicates the amplitude of the radar signals, approximate spatial scale is reported (5 times vertical exaggeration). The view is oriented from the top left corner to the bottom left corner of the context map of Figure 5 (NW to SE). The curved reflections associated with the antiform can be followed along the profile, dipping under the *radar facie* associated with the loose sediments, onlapping over the bedrock at the base of the slope. Visualizing the two radar data profiles in three-dimension allows to observe aspects which are impossible to render in two dimensions, as for example the attitude of the signal associated with the bedrock reflections at the crossing of the two radargrams. Color images are available online.

The data show several GPR *facies*, including (1) high-amplitude low-frequency reflectors, (2) lower amplitude high-frequency reflectors, (3) attenuated areas, and (4) diffraction patterns. We interpret these data to be related to specific geological features as follows: (1) sedimentary layering, (2) bedrock layers, (3) presence of conductive soils (compositional changes), and (4) presence of pebbly materials in the shallow subsurface (change in terrain texture). The spatial relationship of these facies is the result of the sequence of geological processes that occurred throughout the geological history in this region.

The capability of locating shallow subsurface structures by GPR has significant relevance to astrobiology studies, particularly those that search for habitable past environments on Mars.

Since the surface of Mars is hostile to life, with radiation, cold temperatures, and oxidative chemistry destroying organic matter, GPR experiments open a view into the shielded shallow subsurface. Buried geological structures and their relative emplacement processes, when indicating habitable conditions, may be linked to the potential evolution of life on the planet, or possibly host biomass. Moreover, it is also possible that the shallow subsurface of Mars hosts ice, liquid water, and oxygen (Stamenkovic *et al.*, 2018).

As a noninvasive geophysical method, radar sounding offers an indirect measurement of the geological setting of subsurface structures, requiring the conversion of echo returns from time to depths with an estimate of the propagation speed of waves in the subsurface. Coupling a radar with an *in situ* investigation, such as an explorative drilling campaign, will provide direct access to subsurface rocks, thereby enabling the validation of radar data (Tillmann and Wunderlich, 2014).

Such procedures have been planned for the ESA-Roscosmos ExoMars 2022 mission, where the WISDOM radar and Ma_MISS spectrometer within the drill will coordinate noninvasive radar and *in situ* compositional observations to depths of 2 m in the subsurface of the ancient terrains of Oxia Planum (Ciarletti *et al.*, 2017; De Sanctis *et al.*, 2017; Vago *et al.*, 2017). After the drilling, the spectrometer will detect the composition of the rocks being investigated. From the composition of the different layers, it will be possible to improve the quality of radar data processing, deriving a more accurate model of propagation of the electromagnetic waves in the ground. Moreover, GPR data will be critical for the selection of the drilling site, targeting interesting reflectors, or indicating where drilling could be cumbersome, as in the case of the presence of boulders in the terrain, hampering continuous drilling to depth. This is also true in the case of a mission that will prepare samples to be returned to Earth, for example, NASA Mars 2020, where the radar will assist the selection of the best location for extracting unweathered samples.

Using ScanMars in the selection of a drilling site for astrobiology purposes would avoid explorative drilling where the dense diffraction pattern of radar signals suggests the presence of buried boulders in the shallow subsurface (Fig. 7). A possible target for drilling could be the layered bedrock at the outcrop along the slope (Fig. 8) or just over the onlapping layers (Fig. 8, panel I, white arrow) so that the drilling would investigate or sample more terrains down to 1–1.5 m, for example, the recent layered deposits, their contact with the bedrock and the layered rock, which potentially host traces of present or past life. Compositional data obtained from this explorative drilling could then be applied to the processing of radar data for more accurate depth-converted profiles.

Another feature of the radar technique relevant to astrobiology is its capability to detect interfaces between materials with very high dielectric contrasts, such as the interface between rock and water or air (Annan, 2002), enabling the mapping of the water table or cavities, such as lava tubes or ice caves (Clifford, 1993; Cushing *et al.*, 2007; Williams *et al.*, 2010).

Results from our ScanMars and forthcoming experiments onboard Mars2020 and ExoMars 2022 support the idea that GPR is a key instrument for current and future landed planetary missions focused on the search for signs of present or past life on Mars, sample return, and human exploration.

Our experiment has successfully operated thanks to the enthusiastic effort of all the personnel of the mission, from the field crew to the operations and science teams.

Working on the definition of procedures for the operation of ScanMars by nonspecialized personnel in a limited timeslot of a few months has been shown to be particularly challenging. To keep operations practicable by the analog astronauts, we had to preselect the operating modes for the radar (spatiotemporal resolution, setup of sampling time window); however, these are usually optimized by experts in the field depending on the particular terrain. Ideally, having a trained field geophysicist in the field would minimize the risk of losing precious time during the analog campaign by selecting the acquisition strategy *on site*. Moreover, the presence of a field geologist would also support the scientific experiments through observation of the geologic context at the surface, which in our work was shown to be fundamental in interpreting the data with confidence (see interpretation of profile n. 31).

The typical AMADEE mission lifecycle lasts $\sim$2 years, which is extremely quick compared with actual missions, where just the landing site selection itself takes more than 5 years (Golombek *et al.*, 2012). This represents an opportunity to accomplish a complete analog mission project within a relatively short timeline, which gives the opportunity to improve the general technical and procedural aspects over subsequent mission cycles.

From our experience within this tight schedule, we have found that there is still space to optimize the time devoted to the geoscientific characterization of the analog landing area. To improve future AMADEE missions, it would be advisable to allocate more time for scientific familiarization with the simulated landing site, starting as soon as possible in the mission timeline, which would allow the mission team to discuss the scientific campaign. The geoscientific knowledge of the landing site from remote sensing has been an essential aspect since the beginning of planetary exploration. Being a time-consuming, iterative, and interpretative task, the sooner the scientific reconnaissance of the landing site begins, the more time will be available for the planning of the scientific campaign. Possible enhancement of future AMADEE missions might involve organizing a single or multiday scientific workshop focused on the geoscientific characterization of the simulated landing site or region as soon as the field-study area is known.

AMADEE-18 excelled in design, planning, and the deployment of the remote sensing data distribution to the team. Remote-sensing data were made available as soon as possible by the OeWF team, and the dissemination of data through interoperable GIS web-services was invaluable and facilitated planning and communicating ScanMars transect location seamlessly with the whole mission team.

Another aspect for improvement that arose during ScanMars was the difficulty in operating instruments that are not customized for use in an analog space mission. The use of off-the-shelf commercial equipment introduced certain complexities during operation by analog astronauts in bulky space suits, such as difficulties in assembly, handling the hardware, and the physical operation of the instrument. Building a specific instrument for an analog mission would introduce unmanageable budget costs and would be impossible to realize in the timeframe proposed by the AMADEE mission model. A viable solution would be to study this aspect in detail, for example by a dedicated task or activity that locates critical aspects with the intent to develop possible modifications to commercial hardware, and improve the ergonomics for use by analog astronauts in spacesuits.

The AMADEE-18 ScanMars experiment gathered a wide pool of experience from the beginning to the end of the mission and added to similar experiments (Groemer *et al.*, 2014, 2016) and improved aspects related to the compactness of instruments, pre-mission training, and remote science support operations during the mission.

The new scientific data and technical knowledge gained during the mission have increased our research and operational competence and will improve the quality and effectiveness of future surveys.

5. Conclusions

This work describes the ScanMars experiment onboard AMADEE-18 analog mission, held in Oman in February 2018. The ScanMars scientific field campaign returned radar data from $\sim$2000 m of profiles acquired over several target sites. We provided procedures and trained analogue astronauts, who, without previous experience in this field, were able to run the experiment along the planned transects in their spacesuits at the simulated landing site. The day-by-day analysis of the collected data allowed us to improve the procedures and the tuning of the instrument during the simulated mission. Herein, we presented the results from one of the sites explored, where the radar imaged the subsurface down to 4 m in depth, showing signals that allowed for the detection of folded layered rocks, alluvial deposits, and shallow debris, and describing the geology of relatively recent loose terrains emplaced over an older deformed bedrock. We successfully demonstrated that GPR techniques are important tools for paleogeographic reconstructions, which is relevant to astrobiological studies where paleo-surfaces unexposed to space radiation represent potential scientific targets for biosignature searches.

The AMADEE timeline model represents an interesting opportunity to accomplish a complete analog mission within a time frame of around 2 years from mission to mission, requiring and stimulating cooperativeness among the mission team.

The experience gained from the experiment revealed some aspects of the project that could be improved in the future, specifically the need for a longer preliminary geoscientific study of the landing site, the presence of a geoscientist in the astronaut crew or a longer and more geoscience-focused training program, and the introduction of a study devoted to increase the ergonomics of the instruments by the use of personnel in spacesuits.

The experiment successfully fulfilled its main task of bringing an astronaut-operated GPR to an analog landing site, thereby assisting the characterization of the subsurface geology of the target area.

ScanMars adds to a growing list of analog mission experiments that contribute to the design of future planetary surface exploration programs, the search for signs of present or past life, preparation for sample return, and human space exploration.

Acknowledgments

We are grateful to Barbara Cavalazzi and Keyron Hickman-Lewis for their comments and discussions on the astrobiological aspects of this research. We thank Trent Hare for edits and suggestions.

Author Disclosure Statement

No competing financial interests exist.

Funding Information

No specific funding has been received for this research.

References

Abercromby AFJ, Chappell SP, and Gernhardt ML (2013) Desert RATS 2011: human and robotic exploration of near-Earth asteroids. *Acta Astronaut* 91:34–48.

Abrevaya XC, Anderson R, Giada A, *et al.* (2016) The Astrobiology Primer 2.0. *Astrobiology* 16:561–53.

Annan AP (1999) *Practical Processing of GPR Data*, Sensors and Software Inc., Mississauga, ON, Canada.

Annan AP (2001) *Ground-Penetrating Radar Workshop Notes*, Sensors and Software Inc., Mississauga, ON, Canada, 192 p.

Annan AP (2002) GPR—history, trends, and future developments. *Subsurf Sens Technol Appl* 3:253–270.

Annan AP and Davis JL (1976) Impulse radar sounding in permafrost. *Radio Sci* 11:383–394.

Arcone SA (1996) High resolution of glacial ice stratigraphy: a ground penetrating radar study of Pegasus Runway, McMurdo Station, Antarctica. *Geophysics* 61:1653–1663.

Arcone SA, Spikes VB, and Hamilton GS (2005) Phase structure of radar stratigraphic horizons within Antarctic firn. *Ann Glaciol* 41:10–16.

Beaton KH, Chappell SP, Abercromby AFJ, *et al.* (2018) Intra-EVA space-to-ground interactions when conducting scientific fieldwork under simulated mars mission constraints. *Proceedings of IEEE Aerospace Conference 2018*, March 3–10, 2018, Big Sky, MT, USA. Available online at https://ntrs.nasa.gov/search.jsp?R=20170005905 (last accessed February 1, 2020).

Beres M, Huggenberger P, Green AG, and Horstmeyer H (1999) Using two- and three-dimensional georadar methods to characterize glaciofluvial architecture. *Sediment Geol* 129: 1–24.

Bessone L, Sauro F, and Stevenin H (2015) Training safe and effective spaceflight operations using terrestrial analogues. In: *Space Safety is No Accident*. Edited by T Sgobba and I Rongier, Springer, Cham.

Binsted K, Hunter J, Halpern B, *et al.* (2013) HI-SEAS: a long-duration human spaceflight analog in Hawaii. In *Proceedings of the 64th International Astronautical Congress, Space Life Sciences Symposium, Session: Behaviour, Performance and Psychosocial Issues in Space*, Beijing, China.

Binsted K, Bedwell W, Caldwell B, *et al.* (2015) Preliminary results on team function and performance from Hawaii Space Exploration Analog and Simulation (HI-SEAS), *Human Research Program Investigators Workshop*, Houston, TX, USA.

Boisson J, Heggy E, Clifford SM, *et al.* (2011) Radar sounding of temperate permafrost in Alaska: analogy to the Martian midlatitude to high-latitude ice-rich terrains, *J Geophys Res* 116:E11003.

Bradford JH, Harper JT, and Brown J (2009a) Complex dielectric permittivity measurements from ground-penetrating radar data to estimate snow liquid water content in the pendular regime. *Water Resour Res* 45:W08403.

Bradford JH, Nichols J, Mikesell TD, *et al.* (2009b) Continuous profiles of electromagnetic wave velocity and water content in glaciers: an example from Bench glacier, Alaska, USA. *Ann Glaciol* 50:1–9.

Bristow CS and Jol HM (2003) GPR in sediments: advice on data collection, basic processing and interpretation, a good practice guide. In: *Ground Penetrating Radar in Sediments*, edited by CS Bristow and HM Jol, Geological Society Special Publication Vol. 211, pp. 1–7.

Bruzzone L, Plaut JJ, Alberti G, *et al.* (2013) RIME: radar for icy moon exploration. In *2013 IEEE International Geoscience and Remote Sensing Symposium*—IGARSS, pp. 3907–3910. doi: 10.1109/IGARSS.2013.6723686

Butterworth S (1930) On the theory of filter amplifiers. *Exp Wireless Wireless Eng* 7:536–541.

Cannon HN, Stoker CR, Dunagan SE, *et al.* (2007) MARTE: technology development and lessons learned from a Mars drilling mission simulation. *J Field Robotics* 24:877–905.

Casas A, Cosentino P, Fiandaca G, *et al.* (2018) Non-invasive geophysical surveys in search of the Roman Temple of Augustus under the Cathedral of Tarragona (Catalonia, Spain): a case study. *Surv Geophys* 39:1107–1124.

Caudill MC, Pontefract A, Osinski GR, *et al.*, and the CanMars Team (2019) CanMars mission Science Team operational results: implications for operations and the sample selection process for Mars Sample Return (MSR). *Planet Space Sci* 172:43–56.

Cavalazzi B, Barbieri R, Gómez F, et al (2019). The Dallol Geothermal Area, Northern Afar (Ethiopia)—an exceptional planetary field analog on Earth. *Astrobiology* 19:553–578.

Chopra S and Marfurt KJ (2008). Emerging and future trends in seismic attributes. *Leading Edge* 27:298–318.

Ciarletti V, Clifford S, Plettemeier D, *et al.*, and WISDOM Team (2017) The WISDOM radar: unveiling the subsurface beneath the ExoMars rover and identifying the best locations for drilling. *Astrobiology* 17:565–584.

Cinti FR, Pauselli C, Livio F, *et al.* Integrating multidisciplinary, multiscale geological and geophysical data to image the Castrovillari Fault (northern Calabria, Italy). *Geophys J Int* 203:1847–1863.

Clifford SM (1993) A model for the hydrologic and climatic behavior of water on Mars. *J Geophys Res* 98:10973–11016.

Colucci RR, Fontana D, Forte E, *et al.* (2016) Response of ice caves to weather extremes in the southeastern Alps, Europe. *Geomorphology* 261:1–11.

Cushing GE, Titus TN, Wynne JJ, *et al.* (2007) THEMIS observes possible cave skylights on Mars. *Geophys Res Lett* 34: 17201.

Daniels DJ (2004). *Ground Penetrating Radar. Radar, Sonar &Navigation*, Institution of Engineering and Technology, IEE Press, London, 752 pp.

Davis JL and Annan AP (1989) Ground-penetrating radar for high-resolution mapping of soil and rock stratigraphy. *Geophys Prospect* 37:531–551.

Del Gobbo C, Colucci RR, Forte E, *et al.* (2016) The Triglav Glacier (South-Eastern Alps, Slovenia): volume estimation, internal characterization and 2000–2013 temporal evolution by means of ground penetrating radar measurements. *Pure Appl Geophys* 173:2753–2766.

De Sanctis MC, Altieri F, Ammannito E, *et al.*; and the Ma_-MISS Team (2017) Ma_MISS on ExoMars: mineralogical characterization of the martian subsurface. *Astrobiology* 17: 612–620.

Ding CY, Cai YZ, Xiao ZY, *et al.* (2020) A rocky hill on the continuous ejecta of Ziwei crater revealed by the Chang'e-3 mission. *Earth Planet Phys* 4:1–6.

Dorizon S, Ciarletti V, Plettemeier D, *et al.* (2016) Performance validation of the ExoMars 2018 WISDOM GPR in ice caves, Austria. *Planet Space Sci* 120:1–14.

Ercoli M, Pauselli C, Forte E, *et al.* (2012) A multidisciplinary geological and geophysical approach to define structural and hydrogeological implications of the Molinaccio spring (Spello, Italy). *J Appl Geophys* 77:72–82.

Ercoli M, Pauselli C, Frigeri A, *et al.* (2014) 3-D GPR data analysis for high-resolution imaging of shallow subsurface faults: the Mt Vettore case study (Central Apennines, Italy). *Geophys J Int* 198:609–621.

Ercoli M, Pauselli C, Cinti FR, *et al.* (2015). Imaging of an active fault: comparison between 3D GPR data and outcrops at the Castrovillari fault, Calabria, Italy. *Interpretation* 3: SY57.

Ercoli M, Brigante R, Radicioni F, *et al.* (2016) Inside the polygonal walls of Amelia (Central Italy): a multidisciplinary data integration, encompassing geodetic monitoring and geophysical prospections. *J Appl Geophys* 127:31–44.

ESA (2019) Planetary Analogue Geological and Astrobiological Exercise for Astronauts. https://www.esa.int/Our_Activities/Human_and_Robotic_Exploration/Caves/What_is_Pangaea (last accessed 01.02.20).

Fang G, Zhou B, Ji Y-C, *et al.* (2014) Lunar Penetrating Radar onboard the Chang'e-3 mission. *Res Astron Astrophys* 14: 1607–1622.

Farr TG, Arcone S, Arvidson RW, *et al.* (2002) Terrestrial Analogs to Mars. In *The Future of Solar System Exploration (2003–2013)—Community Contributions to the NRC Solar System Exploration Decadal Survey*, edited by MV Sykes, ASP Conference Proceedings, Astronomical Society of the Pacific, San Francisco, pp. 35–76.

Ferrari M, De Angelis S, De Sanctis MC, *et al.* (2018) Spectral characterization of the Ma_MISS instrument on board the ExoMars 2020 rover. *European Planetary Science Congress Abstracts* Vol. 12, Berlin, Germany, EPSC2018-859.

Fisher E, McMechan GA, and Annan AP (1992) Acquisition and processing of wide-aperture ground-penetrating radar data. *Geophysics* 57:495–504.

Forte E, Pipan M, Casabianca D, *et al.* (2012). Imaging and characterization of a carbonate hydrocarbon reservoir analogue using GPR attributes. *J Appl Geophys* 81:76–87.

Forte E, Dossi M, Colucci RR, *et al.* (2013) A new fast methodology to estimate the density of frozen materials by means of common offset GPR data. *J Appl Geophys* 99:135–145.

Godio A and Rege RB (2016) Analysis of georadar data to estimate the snow depth distribution. *J Appl Geophys* 129:92–100.

Godio A, Forte E, Pipan M, *et al.* (2015) An overview of GPR investigation in the Italian Alps. *First Break* 33:61–67.

Golombek M, Grant J, Kipp D, *et al.* (2012) Selection of the Mars Science Laboratory Landing Site. *Space Sci Rev* 170: 641–737.

Gorin GE, Racz LG, and Walter MR (1982) Late Precambrian-Cambrian sediments of Huqf Group, Sultanate of Oman. *AAPG Bullet* 66:2609–2627.

Grant JA and Schultz PH (1992) Ground-penetrating Radar as a Tool for Investigating Near-Surface Stratigraphy on Mars. In *Workshop on Innovative Instrumentation for the in situ Study of Atmospherie-Surface Interactions on Mars*, Part 1. A Lunar and Planetary Institute Workshop held at the Max-Planck-Institute, Mainz, Germany, October 8–9, 1992. Edited by B Fegley Jr and H Waenke. LPI Technical Report 92-07, Part 1, published by Lunar and Planetary Institute, Houston, TX, p. 5.

Grant JA, Schutz AE, and Campbell BA (2003) Ground-penetrating radar as a tool for probing the shallow subsurface of Mars. *J Geophys Res (Planets)* 108:5-1.

Grasmueck M (1996) 3-D Ground-Penetrating Radar applied to fracture imaging in gneiss. *Geophysics* 61:1050.

Groemer G (2014) Simulating Mars on Earth. *Astrobiology* 14: 357–359.

Groemer G (2018) AMADEE-18 Mission Report, OeWF, 149 pp. https://oewf.org/en/portfolio/amadee-18/ (last accessed 01.02.20).

Groemer G, Frischauf N, Soucek A, *et al.* (2007) AustroMars—a simulated high- fidelity human Mars analogue mission, Mars2030—AustroMars Science Workshop. In *Proceedings of the Conference Held at the University of Salzburg*, edited by G. Groemer, September 24–26, 2006, Austrian Space Forum, Innsbruck, Austria, pp. 4–12.

Groemer G, Soucek A, Frischauf N, *et al.* (2014) The MARS2013 Mars analog mission. *Astrobiology* 14:360–376.

Groemer G, Losiak A, Soucek A, *et al.* (2016) The AMADEE-15 Mars simulation. *Acta Astronaut* 129:277–290.

Groemer G, Gruber S, Uebermasser S, *et al.* (2020) The AMADEE-18 Mars Analog Expedition in the Dhofar region of Oman. *Astrobiology* 20:1276–1286.

Gruber S, Grömer G, Haider O (2019) Inspiring the next generation through the AMADEE-18 MARS analog simulation. *Acta Astronaut* 164:204–211.

Hamran S, Berger T, Brovoll S, *et al.* (2015) RIMFAX: A GPR for the Mars 2020 rover mission. In *8th International Workshop on Advanced Ground Penetrating Radar (IWAGPR)*, Florence, Italy. DOI: 10.1109/IWAGPR.2015.7292690

Hamran SE, Amundsen HEF, Asak L, *et al.* (2016) The RIMFAX GPR Instrument Development for the Mars 2020 Rover Mission. In *3rd International Workshop on Instrumentation for Planetary Mission*, Pasadena, USA, 1980, 4031.

Häuplik-Meusburger S, Binsted K, Bassingthwaighte T, *et al.* (2017) Habitability studies and full-scale simulation research: preliminary themes following HISEAS mission IV. In *Conference on Environmental Systems,* Charleston, USA, ICES-2017-138.

Huggenberger P (1993) Radar facies: recognition of facies patterns and heterogeneities within Pleistocene Rhine gravels, NE Switzerland. In *Braided Rivers*. edited by JL Best and CS Bristow. Geol Soc London Spec Publ 75:163–176.

Imhof B, Hoheneder W, Ransom S, *et al.* (2015) Moonwalk—human robot collaboration mission scenarios and simulations. In *Proceedings of the AIAA SPACE 2015 Conference and Exposition*, Pasadena, p. 4531.

Jol HM (2009) *Ground Penetrating Radar Theory and Applications*, Elsevier, Amsterdam, The Netherlands, p. 544.

Knightly JP, Clarke JDA, Rupert S, *et al.* (2018) Summary of field investigations from the MARS 160 analog mission in Utah and Devon Island [abstract 2813]. In *50th Lunar and Planetary Science Conference,* Texas.

Kofman W, Herique A, Barbin Y, *et al.* (2015). Properties of the 67P/Churyumov-Gerasimenko interior revealed by Consert radar. *Science* 349:aab0639.

Kowalczyk S, Cabalski K, and Radzikowski M (2017). Application of geophysical methods in the evaluation of anthropogenic transformation of the ground: a case study of the Warsaw environs, Poland. *Eng Geol* 216:42–55.

Lalla EA, Cote K, Hickson D, *et al.* (2020) Laboratory analysis of returned samples from the AMADEE-18 Mars analog mission. *Astrobiology* 20:1303–1320.

Liner CL (1997) Application of GPR to a site investigation involving shallow faults. *Leading Edge* 16:1649–1651.

Liu B, Tan C, Yu X, *et al.* (2019) Evolution model of a modern delta fed by a seasonal river in Daihai Lake, North China: determined from ground-penetrating radar and trenches. *Front Earth Sci* 13:262–276.

Liu L and Xie X (2013) GPR for geotechnical engineering. *J Geophys Eng* 10, doi: 10.1088/1742-2132/10/3/030201.

Losiak A, Gołebiowska I, Orgel C, *et al.* (2014a) Design and utility optimization of maps for long duration planetary missions. *Astrobiology* 14:417–430.

Losiak A, Gołębiowska I, Orgel C, *et al.* (2014b) Remote science support during MARS2013: testing a mapbased system of data processing and utilization for the future long-duration planetary missions. *Astrobiology* 14:417–430.

Martins Z, Cottin H, Kotler JM, *et al.* (2017) Earth as a tool for astrobiology: a European perspective. *Space Sci Rev* 209: 43–81.

McClymont AF, Green AG, Villamor P, *et al.* (2008) Characterization of the shallow structures of active fault zones using 3-D Ground Penetrating Radar data. *J Geophys Res Solid Earth* 113(B10). doi: 10.1029/2007JB005402.

Neal A (2004). Ground-penetrating radar and its use in sedimentology: principles, problems and progress. *Earth Sci Rev* 66:261–330.

Ono T, Kumamoto A, Yamaguchi Y, *et al.* (2008) Instrumentation and observation target of the lunar radar sounder (lrs) experiment onboard the selene spacecraft. *Earth Planets Space* 60:321–332.

Orgel C, Kereszturi Á, Váczi T, *et al.* (2014) Scientific results and lessons learned from an integrated crewed Mars exploration simulation at the Rio Tinto Mars analogue site. *Acta Astronaut* 94:736–748.

Orosei R, Jordan RL, Morgan DD, *et al.* (2015) Mars Advanced Radar for Subsurface and Ionospheric Sounding (MARSIS) after nine years of operation: a summary. *Planet Space Sci* 112:98–114.

Orosei R, Lauro SE, Pettinelli E, *et al*. (2018) Radar evidence of subglacial liquid water on Mars. *Science* 361:490–493.

Osinski G, Leveille R, Lebeuf M, *et al.* (2006) Terrestrial analogues to Mars and the Moon: Canada's role. *Geosci Canada* 33:175–187.

Osinski GR, Battler M, Caudill CM, *et al.* (2019). The CanMars Mars Sample Return analogue mission. *Planet Space Sci* 66: 110–130.

Pellicer XM, Warren WP, Gibson P, *et al.* (2012) Construction of an evolutionary deglaciation model for the Irish midlands based on the integration of morphostratigraphic and geophysical data analyses. *J Quaternary Sci* 27:807–818.

Phillips RJ, Zuber MT, Smrekar SE, *et al.* (2008) Mars north polar deposits: stratigraphy, age, and geodynamical response. *Science* 320:1182–1185.

Picardi G, Plaut JJ, Biccari D, *et al.* (2005) Radar soundings of the subsurface of Mars. *Science* 310:1925–1928.

Pipan M, Forte E, Guangyou F, *et al.* (2003) High resolution GPR imaging and joint characterization in limestone. *Near Surf Geophys* 1:39–55.

Plaut JJ, Picardi G, Safaeinili A, *et al.* (2007) Subsurface radar sounding of the south polar layered deposits of Mars. *Science* 316:92–95.

Plaut JJ, Safaeinili A, Holt JW, *et al.* (2009) Radar evidence for ice in lobate debris aprons in the mid-northern latitudes of Mars. *Geophys Res Lett* 36:L02203.

Poláčková Šolcová I, Šolcová I, Stuchlíková I, *et al.* (2016) The story of 520 days on a simulated flight to Mars. *Acta Astronaut* 126:178–189.

Porcello LJ, Jordan RL, Zelenka JS, *et al.* (1974) The Apollo lunar sounder radar system. *Proc IEEE* 62:769–783.

Preston LJ and Dartnell LR (2014) Planetary habitability: lessons learned from terrestrial analogues. *Int J Astrobiol* 13:81–98.

Preston LJ, Barber S, and Grady M (2014) *Concepts for Activities in the Field for Exploration*, ESA Contract: 4000104716/11/NL/AF. Available online at https://nebula.esa.int/content/concepts-activities-field-exploration-cafe (last accessed February 1, 2020).

QGIS Development Team (2020) *QGIS Geographic Information System. Open Source Geospatial Foundation Project*. Available online at www.qgis.org (last accessed 25.10.2020).

Rossi AP and van Gasselt S (2018). *Planetary Geology*, Springer. Amsterdam, The Netherlands, 441 p.

Rubinstein H, Sorek-Abramovich R, Shikar A, *et al.* (2019) Mars analogs at Ramon crater region: D-MARS. *50th Lunar and Planetary Science Conference 2019*, vol. 2813, The Woodlands, Texas.

Santin I, Colucci RR, Žebre M, *et al.* (2019) Recent evolution of Marmolada glacier (Dolomites, Italy) by means of ground and airborne GPR surveys. *Remote Sens Environ* 235:111442.

Sauro F, Massironi M, Pozzobon R, *et al.* (2018) Training astronauts for field geology: the ESA PANGAEA Training and PANGAEA-eXtension Testing Analogue [abstract 2083]. In *49th Lunar and Planetary Science Conference,* March 19–23, 2018,.

Schmitt HH (1973) Apollo 17 Report on the Valley of Taurus-Littrow. *Science* 182:681–690.

Searle M (2019) *Geology of the Oman Mountains, Eastern Arabia*, GeoGuide, Springer.

Seu R, Biccari D, Orosei R, *et al.* (2004) SHARAD: the MRO 2005 shallow radar. *Planet Space Sci* 52:157–166.

Seu R, Phillips RJ, Alberti G, *et al.* (2007) Accumulation and erosion of Mars south polar layered deposits. *Science* 317: 1715–1718.

Snook KJ and Mendell WW (2004) The need for analogue missions in scientific human and robotic planetary missions [abstract 2130]. In *XXXV Lunar Planetary Science Conference.*

Solla M, Lorenzo H, Rial FI, *et al.* (2011) GPR evaluation of the roman masonry arch bridge of lugo (Spain). *NDT E Int* 44:8.

Stamenkovic V, Ward LM, Mischna M, *et al.* (2018) O_2 solubility in Martian near-surface environments and implications for aerobic life. *Nat Geosci* 11:905–909.

Steele A, Amundsen HEF, Fogel M, *et al.*, and Amase 2010 Team (2011) The Arctic Mars Analogue Svalbard Expedition (AMASE) 2010. In *42nd Lunar and Planetary Science Conference*, March 7–11, 2011, The Woodlands, Texas. LPI Contribution No. 1608, p.1588.

Stockton AM, Amador ES, Cable ML, *et al.* (2017) Field Exploration and Life Detection Sampling Through Planetary Analogue Sampling (FELDSPAR) [abstract #3637]. In *Astrobiology Science Conference* 2017, LPI Contribution No. 1965.

Stolt RH (1978) Migration by Fourier transform. *Geophysics* 43:23–48.

Stoker CR, Cannon HN, Dunagan SE, *et al.* (2007) The 2005 MARTE Robotic Drilling Experiment in Río Tinto, Spain: objectives, approach, and results of a simulated mission to search for life in the martian subsurface. *Astrobiology* 5:921–945.

Stuurman CM, Osinski GR, Holt JW, *et al.* (2016) SHARAD detection and characterization of subsurface water ice deposits in Utopia Planitia, Mars. *Geophys Res Lett* 43:9484–9491.

Su Y, Fang GY, Feng, JQ, *et al.* (2014) Data processing and initial results of Chang E-3 lunar penetrating radar. *Research in Astronomy and Astrophysics* 14:1623–1632.

Taner MT, Koehler F, and Sheriff RE (1979) Complex seismic trace analysis. *Geophysics* 44:1041.

Tillmann T and Wunderlich J (2014) Barrier spit accretion model of Southern Sylt, German North Sea: insights from ground-penetrating radar surveys and sedimentological data. *Zeitschrift Geomorphol* 58:137–161.

Vago JL, Westall F, and Pasteur Teams, Landing Site Selection Working Group, and Other Contributors 2017 Habitability on early Mars and the search for biosignatures with the ExoMars Rover. *Astrobiology* 17:471–510.

Vögele T (2016) *MOONWALK—Technologies and Human-Robot Collaboration for Surface Eva Exploration Activities and Training in European Analogue Environments*. Final Project Report. Available online at https://cordis.europa.eu/project/id/607346/reporting (last accessed 1.10.2020).

West MD, Clarke JDA, Laing JH, *et al.* (2010) Testing technologies and strategies for exploration in Australian Mars analogues: a review. *Planet Space Sci* 58:4658–4670.

Williams KE, McKay CP, Toon OB, *et al.* (2010) Do ice caves exist on Mars? *Icarus* 209:358–368.

Williford KH, Farley KA, Stack KM, *et al.* (2018) Chapter 11—the NASA Mars 2020 Rover Mission and the Search for Extraterrestrial Life. In *From Habitability to Life on Mars,* edited by NA Cabrol and EA Grin, Elsevier, Amsterdam, The Netherlands, pp, 275–308.

Yilmaz Öz (2001) Seismic data analysis: processing, inversion, and interpretation of seismic data. In *Investigations in Geophysics No. 10,* Vol. 1 and 2, Society of Exploration Geophysicists, Tulsa, USA, 2027p., ISBN 1-56080-094-1.

Zhao W, Forte E, Pipan M, *et al.* (2013) Ground penetrating radar (GPR) attribute analysis for archaeological prospection. *J Appl Geophys* 97:107–117.

Address correspondence to:
Alessandro Frigeri
Istituto di Astrofisica e Planetologia Spaziali
Istituto Nazionale di Astrofisica
via del Fosso del Cavaliere, 100
I-00133 Rome
Italy

E-mail: alessandro.frigeri@inaf.it

Submitted 20 January 2020
Accepted 6 September 2020

Abbreviations Used

DTM = Digital Terrain Model
EVA = extra-vehicular activity
GIS = Geographic Information System
GPR = ground penetrating radar
MARSIS = Mars Advanced Radar for Subsurface and Ionosphere Sounding
OeWF = Österreichisches Weltraum Forum
RIMFAX = Radar Imager for Mars' Subsurface Exploration
SEIF = Standard Experiment Information Form
SHARAD = Shallow Subsurface Radar
WISDOM = Water Ice and Subsurface Deposit Observation on Mars